Enhanced fluctuation for pinned surface nanobubbles

Zhenjiang Guo and Xianren Zhang*
State Key Laboratory of Organic-Inorganic Composites, Beijing University of Chemical Technology, Beijing 100029, China

(Received 17 August 2019; published 18 November 2019)

By employing molecular dynamics simulations we investigate the fluctuation of surface nanobubbles immersed in liquid phase. Our simulation results indicate that in comparison with the surrounding liquid and nanobubble interior, the vapor-liquid or gas-liquid interface of nanobubbles always exhibits the largest compressibility, demonstrating the enhanced fluctuation for nanobubble interfaces. We also find that vapor surface nanobubbles and gas surface nanobubbles exhibit different fluctuation behaviors. For vapor nanobubbles that appear in overheated pure liquid, both density fluctuation and interface fluctuation are independent on the external pressure since the internal pressure remains constant at a given temperature. For gas nanobubbles that appear in gas supersaturated solution, the density fluctuation monotonously decreases with the increase of gas concentration, while the interface fluctuation shows a nonmonotonic variation. Departure from the intermediate gas concentration with the minimal interface fluctuation would enhance the fluctuation, which may finally lead to nanobubble destabilization. Finally, our simulation results indicate that the complicated interface fluctuation of surface nanobubbles comprises two different modes: interface deformation and interface oscillation, both of which display similar trends as that of the combined interface fluctuation.

DOI: 10.1103/PhysRevE.100.052803

I. INTRODUCTION

Accumulated experimental evidence has demonstrated that surface nanobubbles at the solid-liquid interfaces [1,2] can live for several hours or days [3,4], although the nanosized bubbles would experience high Laplace pressure induced by the highly curved liquid-gas interfaces of the bubbles [5]. The nanobubble stability was explained with contact line pinning [6–8], which prevents the tiny bubbles from shrinking and growing, and with gas supersaturation [9,10]. Owing to the effect of their small size [4], surface nanobubbles with a highly curved vapor-liquid interface often show substantially different properties when compared to their macroscopic counterparts [11]. In particular, it is interesting to investigate how the finite size of a surface nanobubble affects the density and shape (interface) fluctuations, which are empirically supposed to be at the root of nanobubble stability. One might expect a size-dependent density and shape fluctuation for surface nanobubbles since this is analogous to the size effect found for nanofluidics and microfluidics; thermal fluctuations for density, volume, and interface were found to be enhanced as the system size decreases [12–25]. However, the thermodynamic fluctuation of surface nanobubbles, which owns a nanocurved vapor-liquid interface and encapsulated vapor-gas package, to the best of our knowledge, has not been discussed before.

Here, using molecular dynamics (MD) simulations we investigated surface nanobubble fluctuation for the density of encapsulated fluid and for the bubble interface. As demonstrated below, the interfacial fluctuation of surface nanobubbles seems to be related to their stability, and therefore has a significant effect on their potential applications. Our simulation results show that different from the fluctuation of flat interfaces, the interface fluctuation of surface nanobubbles comprises two basic classes of modes: interface deformation and interface oscillation, both of which can be recognized with different order parameters. The two modes, which are necessary and sufficient to describe nanobubble fluctuations, behave differently according to the encapsulated fluids: vapor surface nanobubbles in overheated pure liquid and gas surface nanobubbles in gas supersaturated solution.

II. METHOD

In this work, MD simulations in the isothermal, isostress ($NP_{zz}T$) ensemble were performed by using LAMMPS [26]. A quasi-two-dimensional simulation box in a size of $98.6 \times 6.6 \times H$ [with $x(-49.3, 49.3)$, $y(-3.3, 3.3)$, and $z(0, H)$ in units of σ^3 with σ the molecular diameter] was employed with fluctuating box height H [see Fig. 1(b)], encapsulating a fixed number of Lennard-Jones (LJ) molecules $N = 27\,840$ (including both liquid and gas molecules). Periodic boundary conditions were applied in the x and y directions, while in the z direction two restraining substrates were used [see, e.g., Fig. 1(b)], both of which were made up of frozen solid molecules on a fcc lattice with a lattice parameter of $1.64\,\sigma$. On the top substrate, an external force along the z direction was exerted to maintain the given external pressure, P_{ext} [10], while the bottom substrate was fixed during the simulations. For the bottom substrate a square pore with a width of $L = 49.3\,\sigma$ and a depth of $D = 45.2\,\sigma$ was introduced to pin and thus to stabilize surface nanobubbles.

According to our previous work [10], either overheating or gas supersaturation is able to stabilize surface nanobubbles. Therefore, we differentiate here vapor surface nanobubbles

*zhangxr@mail.buct.edu.cn

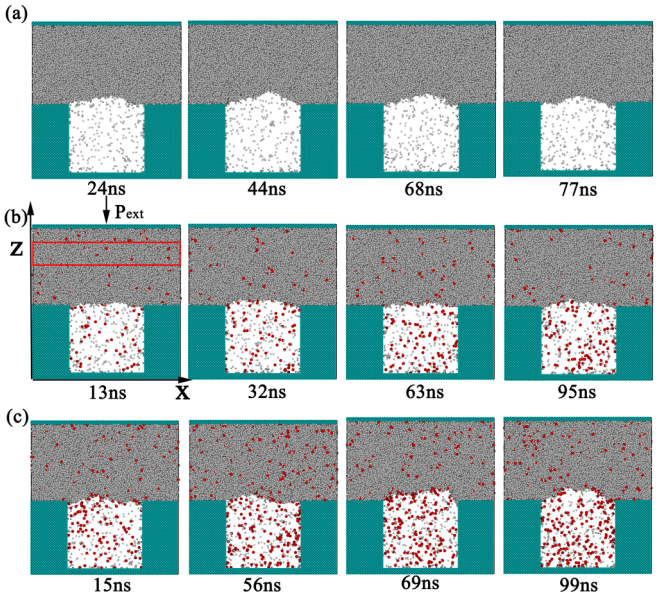

FIG. 1. The representative snapshots for (a) pinned vapor surface nanobubble under an external pressure of 0.0049 and for (b),(c) pinned gas surface nanobubbles at the gas concentrations of (b) 0.01 and (c) 0.02. For gas nanobubbles, $P_{ext} = 0.0122$. In the snapshots, liquid molecules are shown in silver, gas molecules in red, and solid particles in blue. A typical representation of the simulation box is shown in the first snapshot of (b), for which the area marked by the red box shows the reservoir to control the gas concentration in the mixture.

in overheated pure fluid from gas surface nanobubbles in gas supersaturated solution. For the simulations in gas-liquid mixtures, the volume fluctuation of nanobubbles is always accompanied with gas inflow and outflow, which correspondingly change the given gas concentration in the bulk liquid due to the finite size effect. To minimize the finite size effect, a reservoir containing targeted numbers of dissolved gas molecules far from nanobubbles [see the region marked with colored borders in Fig. 1(b)] was introduced to maintain the target gas concentration through performing the identity exchange of liquid and gas molecules in the reservoir. In practice the identity exchange in the reservoir was performed every 0.01 ns.

For all intermolecular interactions, the truncated LJ 12-6 potential was employed (see Table I for LJ parameters) with the characteristic energy parameter ε and the molecular diameter σ, as well as the cutoff distance of 3.2σ. In our simulations, the temperature was always set to $k_BT = 0.85\varepsilon$ with k_B the Boltzmann constant, and the Nosé-Hoover thermostat with a time constant of 0.5 ps was used to control the fluid temperature. The velocity-Verlet algorithm with a time step of 5 fs was used for the integration of equations of motion. We performed the simulations as follows: at first, 27 840 fluid molecules were randomly placed between the bottom and top substrates except the pore; then, a 30 ns MD simulation run was performed at the corresponding saturation pressure for the solvent ($P_{ext} = P_{sat} = 0.0122\,\sigma^3/\varepsilon$, and the units of pressure is hereafter omitted to simplify the description) to equilibrate the system and then changed to other target conditions with another 30 ns run. Finally, a 100 ns simulation was performed for sampling nanobubble fluctuations.

TABLE I. The parameters for Lennard-Jones interaction between different molecules.

Molecules	ε	σ
Liquid-liquid	1.0	1.0
Liquid-gas	0.667	1.0
Liquid-solid at top	0.5	1.0
Liquid-solid at bottom	0.5	1.0
Gas-gas	0.334	1.0
Gas-solid at top	0.188	1.0
Gas-solid at bottom	0.188	1.0

III. RESULTS AND DISCUSSION

For vapor surface nanobubbles in pure liquid, the external pressure exerted on the top substrate P_{ext} was varied to cover the whole pressure range for stable nanobubbles. As demonstrated in Fig. 2(a), vapor surface nanobubbles are stable under a range of external pressures from -0.0024 to 0.0122. Out of the pressure range, destabilization of surface nanobubbles would occur through phase transition or contact line depinning [27]. The representative snapshots of a stable surface nanobubble under the given external pressure of $P_{ext} = 0.0049$ are given in Fig. 1(a). These observations agree with those demonstrated in previous studies, i.e., the stability of the convex nanobubble is induced by contact line pinning [28] and supersaturation [9,10,29].

For gas-liquid mixtures the external pressure was fixed to 0.0122 and the target gas concentration of gas molecules in the reservoir [see Fig. 1(b)], X_{gas}, was varied to explore the condition for the existence of stable gas surface nanobubbles. Here the change of X_{gas} in fact changes the gas supersaturation ξ since $\xi \equiv \frac{X_{gas} - X^s_{gas}}{X^s_{gas}}$. Note that at the given pressure of $P_{ext} = P_{sat} = 0.0122$, the saturated concentration of gas molecules X^s_{gas} is ~ 0.001. Our simulation results show that after $X_{gas} > 0.035$, surface nanobubbles would lose their stability through overcoming the required pinning force or through causing liquid-vapor phase transition. In cases of $X_{gas} = 0.01$ and 0.02, typical snapshots of stable gas nanobubbles are shown in Figs. 1(b) and 1(c), respectively. The figures indicate that a higher gas supersaturation results in a larger bubble height, consistent with the previous theoretic and simulation studies [9,10]. More importantly, Fig. 1 as well as the corresponding Supplemental Material movies S1–S3 [30] demonstrate that the instantaneous morphology of quasi-2D surface nanobubbles occasionally exhibits strong shape fluctuation, with nanobubble surfaces sometimes significantly deviating from the cylindrical shape.

To investigate the density fluctuation of surface nanobubbles, the nanobubble compressibility $C(z) = \frac{\langle |\rho(z) - \langle \rho(z) \rangle| \rangle}{\langle \rho(z) \rangle}$ was calculated. Different from flat interfaces, nanobubbles have a curved vapor-liquid interface that covers a variety of z (the direction perpendicular to the substrate), which would blur the fluctuation behaviors of fluid density in the nanobubble interior. To minimize the effect, only a slice of simulation box

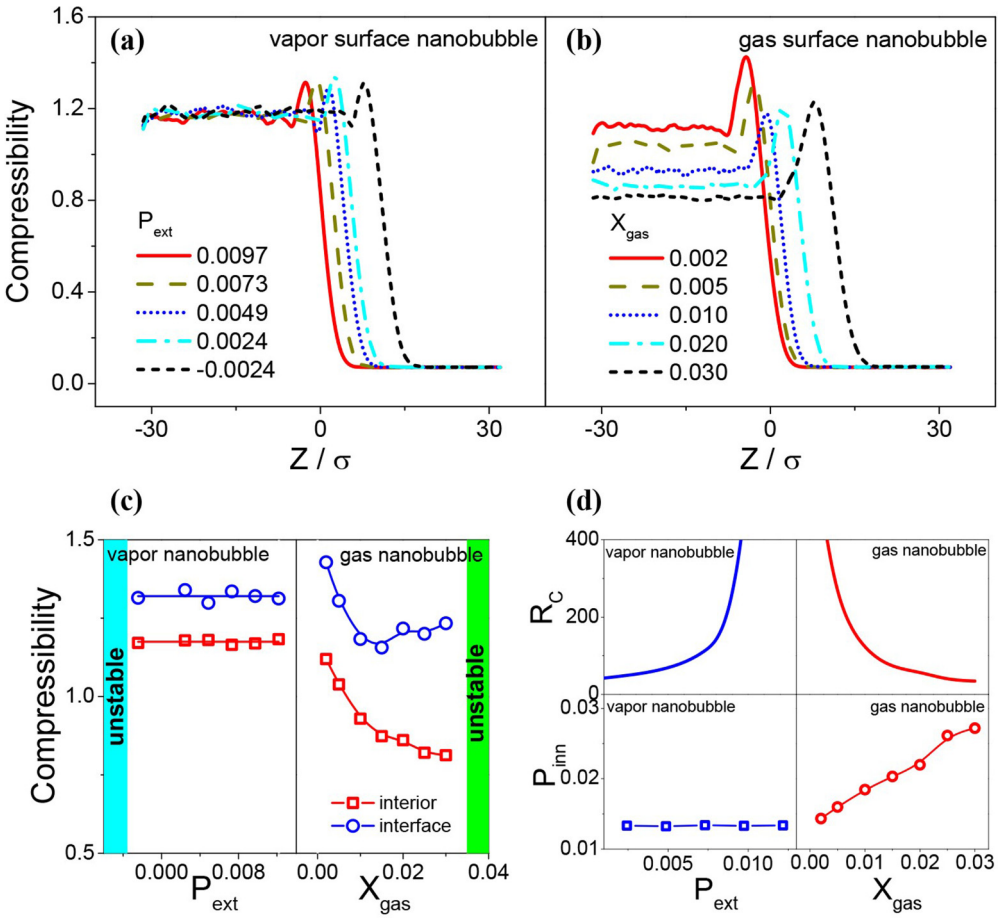

FIG. 2. (a),(b) The compressibility along the z direction (a) for vapor surface nanobubbles and (b) for gas surface nanobubbles. (c) The compressibility for nanobubble interface and that for nanobubble interior. The regions in which nanobubbles become unstable are also given this figure. (d) The calculated curvature radius R_C and internal pressure P_{in} for both types of surface nanobubbles. Here the internal pressure P_{in} was calculated via the state equation of ideal gas.

$(-0.5 \leqslant x \leqslant 0.5)$ was considered to determine $C(z)$, which is shown in Fig. 2(a). As expected, the compressibility of liquid out of both vapor and gas surface nanobubbles is much lower than that for the interior of the bubbles, demonstrating a much more significant density fluctuation for encapsulated gas or vapor. Moreover, another common feature for the two types of nanobbbles is that in comparison with liquid and bubble interior, the vapor-liquid or gas-liquid interface always exhibits the largest compressibility. The large interface compressibility can be interpreted as a consequence of the strong shape fluctuation of nanobubble interfaces, which, as demonstrated below, includes interface deformation and oscillation.

However, vapor and gas nanobubbles in fact show different fluctuation behaviors [Fig. 2(c)]. For vapor nanobubbles, decreasing the external pressure always decreases the curvature radius of the pinned nanobubbles [Fig. 2(d)], but does not significantly alter the compressibility for both vapor in the interior of the bubble and for that of the interface [see Fig. 2(b)]. For gas surface nanobubbles, however, the compressibilities for the bubble interior and that for the interface behave differently as a function of gas supersaturation [Fig. 2(c)], although increasing gas supersatuation results in the decrease of bubble curvature radius (R_C) similar to decreasing external pressure for vapor surface nanobubbles [see Fig. 2(d)]. Increasing gas supersatuation not only reduces the compressibility of the encapsulated gas but also nonmonotonously alters that of the vapor-liquid interface: when $X_{\text{gas}} < 0.015$, the interface compressibility decreases as gas concentration increases. But, as long as it exceeds that threshold value, the compressibility will rise reversely [see Fig. 2(b)].

In order to figure out the key factors affecting thermal fluctuations of vapor and gas nanobubbles, we estimated the internal pressure of the bubbles via employing state equation of ideal gas $P_{\text{in}} = \rho k_B T$, with ρ the number density of vapor or gas molecules inside the nanobubbles. The internal pressures for vapor and gas surface nanobubbles are shown in Fig. 2(d). For vapor surface nanobubbles, although the radius of curvature increases with decreasing applied external pressures [Figs. 2(c) and 3(a)], the internal pressure P_{in} remains unchanged [Fig. 2(d)]. This clearly demonstrates that for vapor nanobubbles the density compressibility depends only on the internal pressure, but is curvature radius and external pressure independent.

For gas surface nanobubbles, increasing gas concentration not only induces the decrease of radius of curvature [Fig. 2(d)], but also sharply increases the internal pressure [Fig. 2(d)], which alters the density compressibility

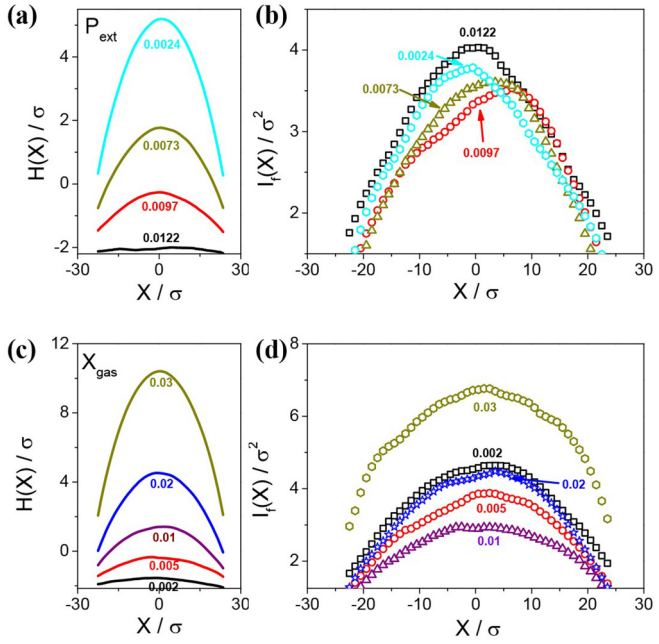

FIG. 3. The average position of nanobubble interfaces $\langle H(x)\rangle$ and the interface fluctuation I_f for (a),(b) vapor surface nanobubble and (c),(d) gas surface nanobubble, respectively.

[Fig. 2(c)]. This means that density compressibility for gas nanobubbles is internal pressure dependent, similar to vapor nanobubbles [see Fig. 2(a)]. The dependence of nanobubble compressibility on bubble internal pressure and that of density fluctuation can be interpreted as follows. By assuming that the vapor or gas encapsulated in quasi-2D surface nanobubbles satisfy the ideal gas law, we can obtain the isothermal compressibility $\beta = -\frac{1}{V}(\frac{\partial V}{\partial P})_T = 1/P_{\text{in}}$, with $P_{\text{in}} = \Delta P + P_{\text{ext}} = \gamma/R + P_{\text{ext}}$ (γ is the surface tension). For vapor nanobubbles, although the radius of curvature R changes with the external pressure, the highly curved vapor-liquid interface leads to an additional pressure $\Delta P = \gamma/R$, which exactly cancels out the variation of P_{ext}. This gives rise to the unchanged internal pressure ($P_{\text{in}} \sim P_{\text{sat}}$) [see Fig. 2(c)], leading to unchanged density compressibility. For gas surface nanobubbles, however, the internal bubble pressure increases with gas concentration in solution according to the Henry's law $P_{\text{in}} = H_{i,\text{solvent}} X_{\text{gas}}$, with $H_{i,\text{solvent}}$ the Henry's law constant. It is the increase of P_{in} that leads to the decrease of compressibility of gas [Fig. 2(c)]. In contrast, the different response of P_{in} to the external perturbation for vapor nanobubbles is ascribed to the quick response of vapor molecules to bubble internal pressure: different from gas molecules, vapor molecules in a nanobubble can rapidly condense onto or evaporate from the vapor-liquid interface as the pressure increases or decreases.

Compared to the density fluctuation, the shape (or interface) fluctuation of surface nanobubbles becomes more complicated, especially for gas nanobubbles. This can be found from the nonmonotonic relation between the compressibility of the interface region and gas concentration X_{gas} [see Fig. 2(c)]. Here, to investigate the shape fluctuation of the vapor-liquid (or gas-liquid) interface [see Figs. 3(b) and 3(d)], we defined an order parameter, $I_f = \langle [H(x) - \langle H(x)\rangle]^2\rangle$, to characterize the interface distortion from its equilibrium interface profile $\langle H(x)\rangle$, in which $H(x)$ is the instantaneous height of the bubble interface at position x (x represents the direction along the base radius) and $\langle H(x)\rangle$ was averaged over the whole simulation run [see, e.g., Fig. 3(a) for vapor nanobubbles and Fig. 3(c) for gas nanobubbles]. Figure 3 clearly indicates that for a pinned surface nanobubble, the part of the vapor-liquid interface far from the contact line exhibits a much stronger local fluctuation than that close to the contact line. It seems that the contact line pinning plays a role in stabilizing nanobubbles through weakening the interface fluctuation, especially at the place close to the contact line. More interestingly, vapor and gas nanobubbles behave differently in interface fluctuation, consistent with Figs. 2(a) and 2(b).

For vapor nanobubbles, the interface fluctuation is nearly independent of the external pressures [Fig. 3(b)], as a result of the unchanged internal pressure [Fig. 2(d)]. In contrast, for gas surface nanobubbles the interface fluctuation shows a nonmonotonic dependence on gas concentration that is proportional to bubble internal pressure according to the Henry's law $P_{\text{in}} = H_{i,\text{solvent}} X_{\text{gas}}$. Before reaching a threshold $X_{\text{gas}} = 0.01$, gas nanobubbles show increasingly weakened interface fluctuation as X_{gas} increases [see Fig. 3(d)], the same trend as that for density compressibility. This implies that in the range of $X_{\text{gas}} < 0.01$, it is the large compressibility of nanobubbles that dominates the interface fluctuation. In this region, increasing the amount of encapsulated gas molecules leads to an increase in internal pressure and thus a decrease in compressibility, which prevents the bubbles from shape fluctuation. When X_{gas} exceeds the threshold, however, increasing X_{gas} leads to an enhanced fluctuation [see Fig. 3(d)] because the high gas pressure in the nanobubble interior reduces the interface tension [31], which in turn softens the interface and promotes the shape fluctuation. Therefore, the opposite effects of gas pressure on compressibility and on surface tension lead to the occurrence of a lowest interface fluctuation at $X_{\text{gas}} = 0.01$.

With detailed inspection on the evolution of instantaneous configurations of nanobubbles, we recognized that the complicated shape fluctuation of surface nanobubbles exhibits different modes, including interface deformation and interface oscillation. Interface deformation, which is also called capillary wave, is the phenomenon that the surface mass points vibrate off balance positions [12,15,16,18,19]. For surface nanobubbles, the equilibrium vapor-liquid interfaces are proven to be spherical cap shaped (it is, in fact, cylindrical cap shaped for the pseudo-2D system we adopted), so that we can create a best-fit circle (circular arc) to the interface at a given simulation time t, which is denoted as $I_{\text{arc}}(x,t)$. Thus, the interface deformation that describes the deviation from the best-fit interface in a cylindrical cap shape is given by $I_d = \langle (\sum_{-L/2}^{L/2} [H(x,t) - I_{\text{arc}}(x,t)]^2 \Delta x) L^{-1}\rangle_t$ with L the base diameter of the nanobubble.

Besides the interface deformation of a pinned nanobubble that deviates from its spherical cap shape, the vapor-liquid (or gas-liquid) interface also exhibits a radial oscillation due to the fluctuation of nanobubble volume. To differentiate from interface deformation, the interface oscillation is defined by the variance of the best-fit arc at a given simulation

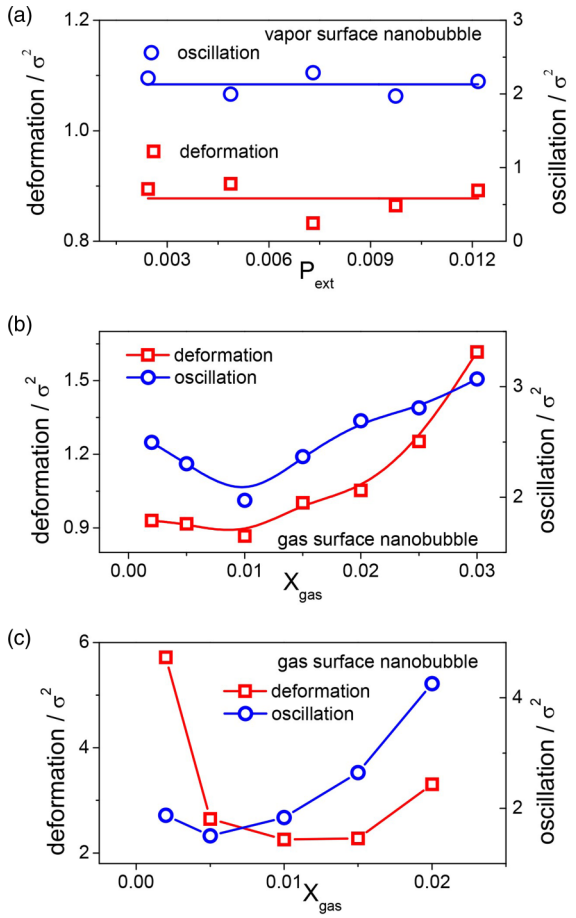

FIG. 4. The deformation and oscillation for the interfaces of (a) vapor surface nanobubbles and those for (b) gas surface nanobubbles. (c) A larger system was employed to investigate the size effect, in which the size of the simulation box was enlarged to $197.3 \times 6.6 \times H$ (in units of σ^3) and the square pore on the bottom substrate was enlarged to a width of $98.6\,\sigma$ and a depth of $61.7\,\sigma$.

time $I_{\rm arc}(x,t)$ with respect to its equilibrium value averaged over the entire simulation run $\langle I_{\rm arc}(x)\rangle$, namely, $I_o = \langle [I_{\rm arc}(x,t) - \langle I_{\rm arc}(x)\rangle]^2\rangle$. The simulation results are shown in Figs. 4(a) and 4(b) for vapor and gas nanobubbles, respectively. Indeed, both kinds of surface nanobubbles show an interface fluctuation mixed by two modes (interface deformation and oscillation).

More importantly, the two modes of shape fluctuation behave differently for vapor and gas nanobubbles, consistent with Fig. 3. For vapor nanobubbles, they are extremely fragile to size and shape fluctuation due to the large compressibility and therefore able to quickly respond to thermal fluctuation. As a consequence of the easily distorted vapor-liquid interfaces, vapor nanobubbles show both strong interface deformation and interface oscillation, both of which are independent of the external pressure [Fig. 4(a)]. For gas nanobubbles, however, both interface deformation and oscillation show nonmonotonic behaviors that are governed by gas supersaturation [Fig. 4(b)]: they first decrease with the gas supersaturation until reaching a minimum at $X_{\rm gas} = 0.01$, after which they increase with $X_{\rm gas}$. When $X_{\rm gas} < 0.01$, the increasing amount of encapsulated gas molecules increases the internal pressure and decreases nanobubble compressibility, which makes the interface more difficult to deform and have a shape closer to spherical cap. Hence, both interface deformation and oscillation become weakened with the increase of $X_{\rm gas}$. For $X_{\rm gas} > 0.01$ corresponding to a higher internal pressure, on the other hand, the decrease of surface tension, which is again induced by increasing internal pressure, dominates the interface fluctuation. In this case, as $X_{\rm gas}$ increases, the decrease of surface tension softens the interface and enhances the interface deformation. Therefore, for gas nanobubbles under the environment of $X_{\rm gas} > 0.01$, it is the reduced surface tension, along with the increased internal pressure, that leads to the strengthened interface deformation and radius (volume) oscillation. In a word, there is a combined effect between gas compressibility and the interface tension that induces the interface deformation and volume oscillation.

We also increased the size of the simulation box to $197.3 \times 6.6 \times H$ (in units of σ^3) and enlarged the square pores, which were designed to stabilize nanobubbles, to a width of $98.6\,\sigma$ and a depth of $61.7\,\sigma$. For the gas nanobubbles in the larger system, the interface fluctuation from MD simulations is shown in Fig. 4(c), which indicates that both interface deformation and interface oscillation change again nonmonotonously with the concentration of dissolved gas. At the range of small $X_{\rm gas}$, increasing $X_{\rm gas}$ leads to the increase of the internal pressure of gas nanobubbles, which prevents the bubbles from shape fluctuation (including both interface deformation and oscillation). When $X_{\rm gas}$ continues to increase, the increasingly high internal pressure, as expected, in turn enhances the interface deformation and oscillation [see Fig. 3(c)], similarly to the observations from the smaller system [see Fig. 3(b)]. This same trend for the two systems of different sizes indicates that the nonmonotonous relationship between $X_{\rm gas}$ (or internal pressure) and interface fluctuation is a common feature for gas nanobubbles. This may partly interpret the experimental observations that most bulk nanobubbles are found in a very small range of size, normally 50–200 nm [32,33]. According to our simulation results, for very large (small) nanobubbles, the sufficiently small (large) internal pressure for gas packets encapsulated in nanobubbles, which is determined by $\Delta P = \gamma/R$, causes enhanced fluctuations, which in turn destabilize the nanobubbles.

IV. CONCLUSION

In summary, the thermodynamic fluctuation for surface nanobubbles was investigated here via MD simulations. First we differentiated vapor nanobubbles formed in overheated pure liquid and gas nanobubbles in gas supersaturated solution since they exhibit totally distinct fluctuation behaviors. Then we differentiated the fluctuation for the density of encapsulated fluid and that for the bubble interface, since our simulation results show that the vapor-liquid or gas-liquid interface of nanobubbles always exhibits the largest compressibility in comparison with the surrounding liquid and the bubble interior. For vapor nanobubbles, both density fluctuation and interface fluctuation are independent on the external pressure under the given temperature. This is because the internal pressure remains unchanged regardless of the applied external pressure. For gas nanobubbles,

however, with increasing the concentration of gas dissolved in solvent, the density fluctuation decreases monotonously. Differently, interface fluctuation shows a nonmonotonic variation with the gas concentration and there exists a minimum value at an intermediate gas supersaturation. Both increasing and decreasing the concentration can enhance the interface fluctuation, which may finally lead to nanobubble destabilization. Further, our simulation results indicate that interface fluctuation of nanobubbles comprises different modes, including interface deformation and interface oscillation. Both of them are combined to constitute the complicated interface fluctuation. The two modes represent, respectively, the deformation of nanobubble interfaces that deviate from the spherical shape, and the radial oscillation of nanobubbles that would lead to the fluctuation of nanobubble volume.

[1] S.-T. Lou, Z.-Q. Ouyang, Y. Zhang, X.-J. Li, J. Hu, M.-Q. Li, and F.-J. Yang, Nanobubbles on solid surface imaged by atomic force microscopy, J. Vac. Sci. Technol. B **18**, 2573 (2000).

[2] N. Ishida, T. Inoue, M. Miyahara, and K. Higashitani, Nano bubbles on a hydrophobic surface in water observed by tapping-mode atomic force microscopy, Langmuir **16**, 6377 (2000).

[3] M. Alheshibri, J. Qian, M. Jehannin, and V. S. Craig, A history of nanobubbles, Langmuir **32**, 11086 (2016).

[4] D. Lohse and X. Zhang, Surface nanobubbles and nanodroplets, Rev. Mod. Phys. **87**, 981 (2015).

[5] P. S. Epstein and M. S. Plesset, On the stability of gas bubbles in liquid-gas solutions, J. Chem. Phys. **18**, 1505 (1950).

[6] X. H. Zhang, D. Y. C. Chan, D. Y. Wang, and N. Maeda, Stability of interfacial nanobubbles, Langmuir **29**, 1017 (2013).

[7] J. H. Weijs and D. Lohse, Why Surface Nanobubbles Live for Hours, Phys. Rev. Lett. **110**, 054501 (2013).

[8] Y. Liu and X. Zhang, Nanobubble stability induced by contact line pinning, J. Chem. Phys. **138**, 014706 (2013).

[9] D. Lohse and X. Zhang, Pinning and gas oversaturation imply stable single surface nanobubbles, Phys. Rev. E **91**, 031003 (2015).

[10] Y. Liu and X. Zhang, A unified mechanism for the stability of surface nanobubbles: Contact line pinning and supersaturation, J. Chem. Phys. **141**, 134702 (2014).

[11] H. Peng, G. R. Birkett, and A. V. Nguyen, Progress on the surface nanobubble story: What is in the bubble? Why does it exist? Adv. Colloid Interface Sci. **222**, 573 (2014).

[12] K. Rane, *Physical Chemistry of Gas-Liquid Interfaces* (Elsevier, Netherlands, 2018).

[13] R. Evans and N. B. Wilding, Quantifying Density Fluctuations in Water at a Hydrophobic Surface: Evidence for Critical Drying, Phys. Rev. Lett. **115**, 016103 (2015).

[14] D. E. Otten, P. R. Shaffer, P. L. Geissler, and R. J. Saykally, Elucidating the mechanism of selective ion adsorption to the liquid water surface, Proc. Natl. Acad. Sci. USA **109**, 701 (2012).

[15] S. N. Jamadagni, R. Godawat, and S. Garde, Hydrophobicity of proteins and interfaces: Insights from density fluctuations, Annu. Rev. Chem. Biomol. **2**, 147 (2011).

[16] K. Wensink and B. Jérôme, Dewetting induced by density fluctuations, Langmuir **18**, 413 (2002).

[17] Z. Toroczkai, G. Korniss, S. D. Sarma, and R. Zia, Extremal-point densities of interface fluctuations, Phys. Rev. E **62**, 276 (2000).

[18] S. W. Sides, G. S. Grest, and M.-D. Lacasse, Capillary waves at liquid-vapor interfaces: A molecular dynamics simulation, Phys. Rev. E **60**, 6708 (1999).

[19] J. Meunier, Liquid interfaces: Role of the fluctuations and analysis of ellipsometry and reflectivity measurements, J. Phys. **48**, 1819 (1987).

[20] F. Detcheverry and L. Bocquet, Thermal Fluctuations in Nanofluidic Transport, Phys. Rev. Lett. **109**, 024501 (2012).

[21] D. Chandler, Physical chemistry: Oil on troubled waters, Nature (London) **445**, 831 (2007).

[22] H. Li and M. Kardar, Fluctuation-Induced Forces Between Rough Surfaces, Phys. Rev. Lett. **67**, 3275 (1991).

[23] A. Ajdari, L. Peliti, and J. Prost, Fluctuation-Induced Long-Range Forces in Liquid Crystals, Phys. Rev. Lett. **66**, 1481 (1991).

[24] F. F. Abraham, On the fluctuation theory for the liquid-vapor interface, Chem. Phys. Lett. **58**, 259 (1978).

[25] D. G. Triezenberg and R. Zwanzig, Fluctuation Theory of Surface Tension, Phys. Rev. Lett. **28**, 1183 (1972).

[26] S. Plimpton, Fast parallel algorithms for short-range molecular dynamics, J. Comput. Phys. **117**, 1 (1995).

[27] Q. Xiao, Y. Liu, Z. Guo, Z. Liu, and X. Zhang, How nanobubbles lose stability: Effects of surfactants, Appl. Phys. Lett. **111**, 131601 (2017).

[28] X. Zhang, H. Lhuissier, C. Sun, and D. Lohse, Surface Nanobubbles Nucleate Microdroplets, Phys. Rev. Lett. **112**, 144503 (2014).

[29] Z. Guo, Y. Liu, Q. Xiao, and X. Zhang, Hidden nanobubbles in undersaturated liquids, Langmuir **32**, 11328 (2016).

[30] See Supplemental Material at http://link.aps.org/supplemental/10.1103/PhysRevE.100.052803 for supporting movies.

[31] O. K. Rice, The effect of pressure on surface tension, J. Chem. Phys. **15**, 333 (1947).

[32] S. H. Oh and J. M. Kim, Generation and stability of bulk nanobubbles, Langmuir **33**, 3818 (2017).

[33] J. Qiu, Z. Zou, S. Wang, X. Wang, L. Wang, Y. Dong, H. Zhao, L. Zhang, and J. Hu, Formation and stability of bulk nanobubbles generated by ethanol–water exchange, ChemPhysChem **18**, 1345 (2017).